Supplementary Material For:

Approaching the isotropic spin-ladder regime: Structure and magnetism of all-pyrazine-bridged

copper(II)-based antiferromagnetic ladders

Jeffrey C. Monroe,[a,*] M. Angels Carvajal,[b] Christopher P. Landee,[c] Mercè Deumal,*[b] Mark M. Turnbull,[a,*] Jan L. Wikaira[d] and Louise N. Dawe[e]

[a] Carlson School of Chemistry and Biochemistry, Clark University 950 Main Street, Worcester MA 01610, USA

[b] Dept. Ciència de Materials i Química Física, & IQCTUB, Universitat de Barcelona, Martí i Franquès 1, Barcelona, E-08028.

[c] Department of Physics, Clark University 950 Main Street, Worcester MA 01610, USA

[d] Department of Chemistry, University of Canterbury, 20 Kirkwood Ave, Upper Riccarton, Christchurch 8041, New Zealand

[e] Dept. of Chemistry and Biochemistry, Wilfrid Laurier University, Waterloo, Ontario, Canada

Section I. Magnetization data, powder X-ray diffraction and additional structure figures.
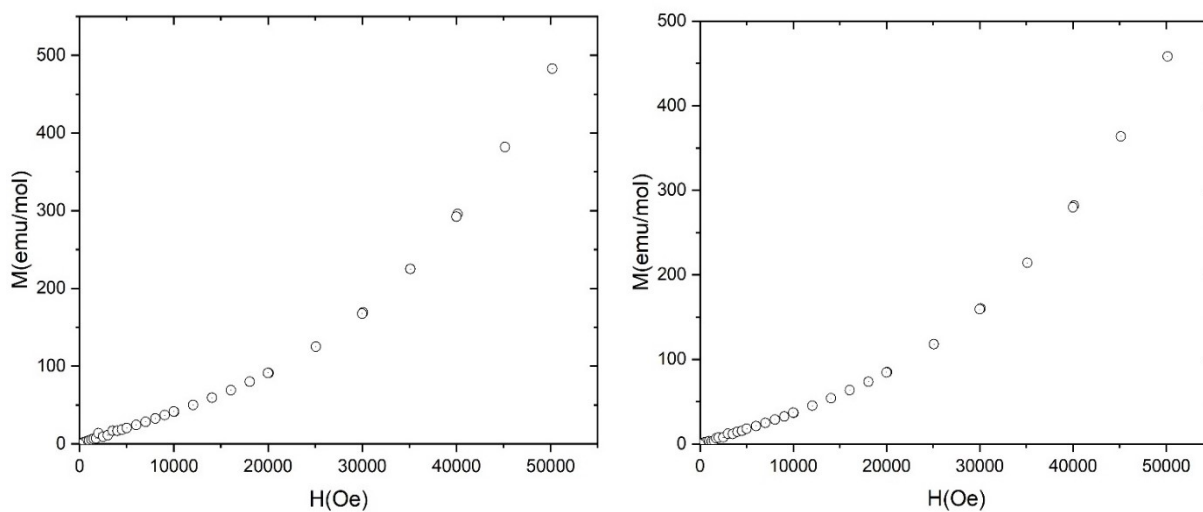

Figure SI.1. Magnetization of **1** (left) and **2** (right) at 1.8 K from 0 to 50 kOe.
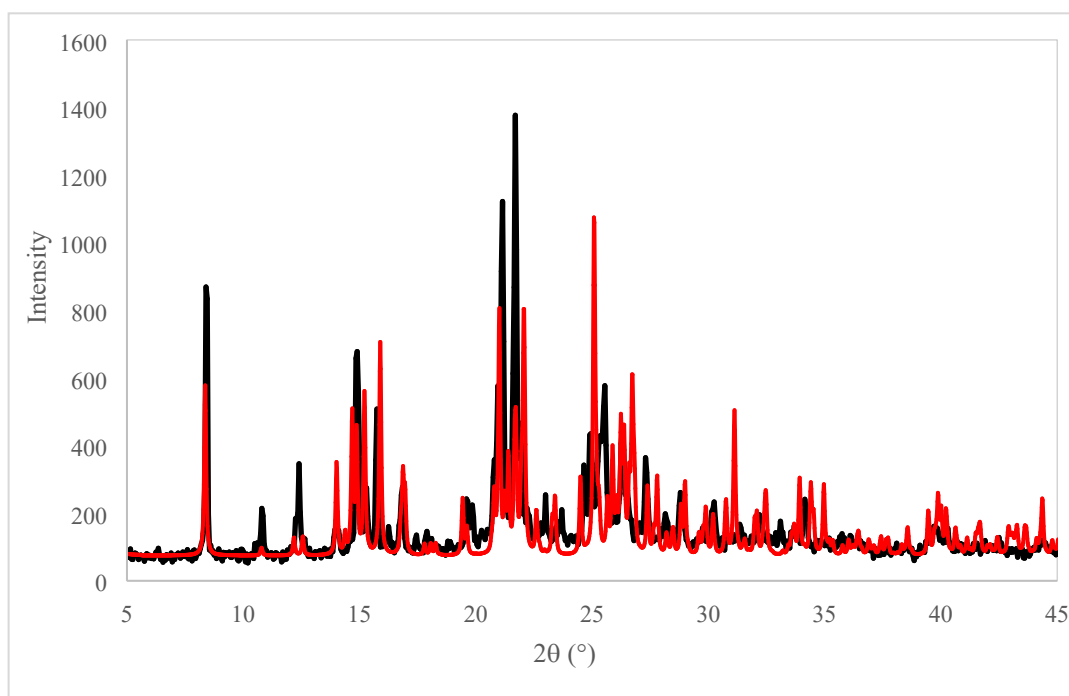

Figure SI.2 - Comparison of experimental (black, room temperature) and calculated (from single-crystal data, red, 120 K) powder patterns for **1**.
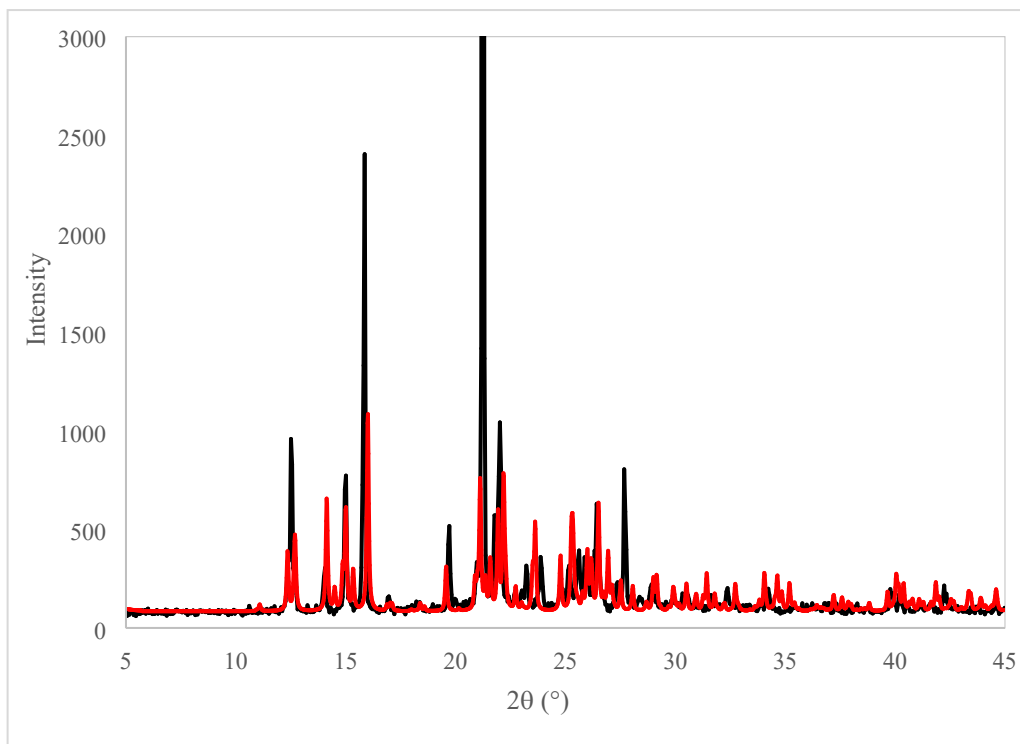
Figure SI.3 - Comparison of experimental (black, room temperature) and calculated (from single crystal data, red, 120 K) powder patterns for **2**.
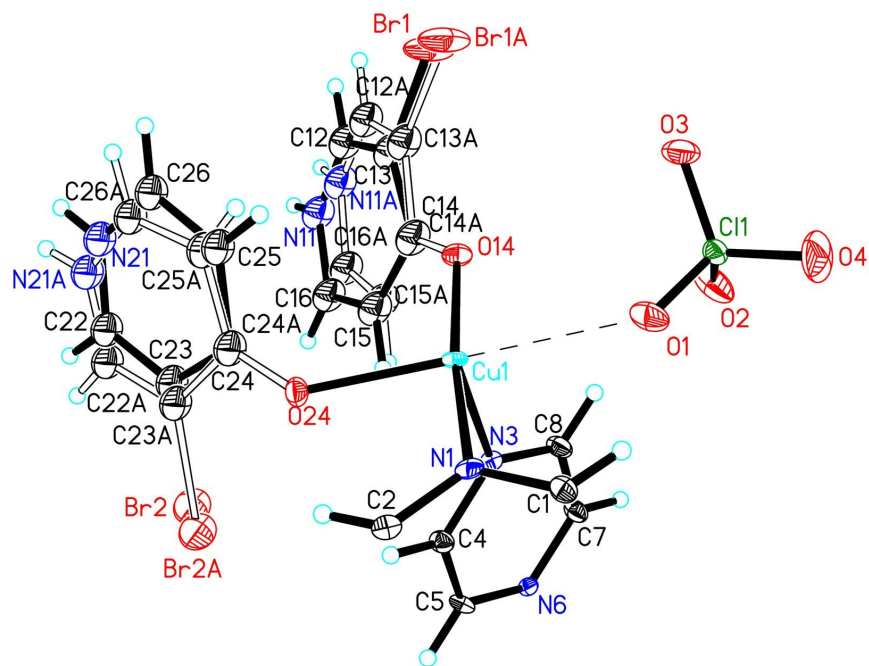

Figure SI.4 The symmetric unit of compound **1** showing the two-site disorder of the pyridone rings. The disordered perchlorate ion has not been included.
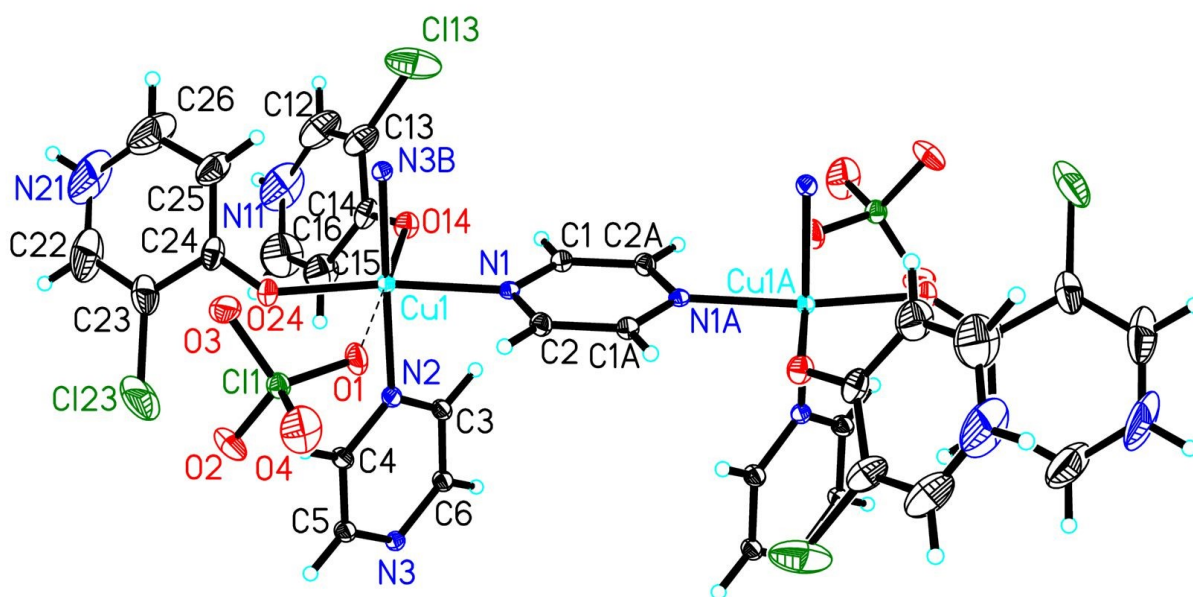
Figure SI.5. A 50% thermal ellipsoid plot of a rung in **2** with the asymmetric unit and one full rung pyrazine ligand labelled. The disordered perchlorate ion are not shown for clarity.

Section II. Additional X-ray Structure Refinement information for compound 1

Due to the one highly disordered perchlorate ion in the lattice, the structure was refined using two different approaches: (i) a four-component model for the ion; and (ii) using the SQUEEZE routine (solvent mask) to remove the highly disordered perchlorate ion. The refinement with the solvent mask has been used in the main document for reporting geometric parameters due to the better bond precision. The model with no mask (the four-component disordered perchlorate ion) is included to support the charge balance and validity of using the solvent mask.

Introduction

Full refinement: The structure contains two fully disordered ligands (0.438(9): 0.562(9) and 0.328(15): 0.672(15) occupancies). Same distances restraints and equal displacement parameter constraints (SHELX SADI and EADP) were used to model these groups, while the pivot atoms (C14/14A and C24/24A) were split but required to occupy the same position (EXYZ).

A fully disordered perchlorate anion is also present. It was modelled with four components which were required to sum to a total of 1.0 (SHELX SUMP; yielding occupancies of 0.280(6), 0.184(5), 0.173(5) and 0.363(5)). Same distances and equal displacement parameter restraints and constraints (SHELXL SADI and EADP) were used to model this anion.

Experimental

A suitable crystal of $C_{16}H_{14}Br_2Cl_2CuN_5O_{10}$ (**1**) was selected and collected on a SuperNova, Dual Atlas diffractometer. The crystal was kept at 120.01(10) K during data collection. Using Olex2 [1], the structure was solved with the SHELXT [2] structure solution program using Intrinsic Phasing and refined with the SHELXL [3] refinement package using Least Squares minimisation. (Note: the two refinements employed the same data set.)

1. Dolomanov, O.V.; Bourhis, L.J.; Gildea, R.J.; Howard, J.A.K.; Puschmann, H. *J. Appl. Cryst.* **2009**, *42*, 339-341.
2. Sheldrick, G. M., *Acta Crystallogr A* **2008,** *64*, 112-22.
3. Sheldrick, G.M. *Acta Cryst.* **2015,** *C71*, 3-8.

Crystal Data for $C_{16}H_{14}Br_2Cl_2CuN_5O_{10}$ (M =730.58 g/mol): monoclinic, space group P2$_1$/c (no. 14), a = 21.4129(7) Å, b = 6.8466(2) Å, c = 16.6158(6) Å, β = 99.172(3)°, V = 2404.83(14) Å^3, Z = 4, T = 120.01(10) K, μ(MoKα) = 4.516 mm^{-1}, $Dcalc$ = 2.018 g/cm^3, 14769 reflections measured (6.616° $\leq$ 2 θ $\leq$ 51.362°), 4578 unique (3896 with I > 2σ(I); R_{int} = 0.0347, R$_{sigma}$ = 0.0359) which were used in all calculations. The final R_1 was 0.0634 (I > 2σ(I)) and wR_2 was 0.1479 (all data).

Solvent mask: In the treatment of the structure via the PLATON SQUEEZE routine, 218 electrons were recovered from a volume of 369 Å^3, accounting for the badly disordered perchlorate anion. This refinement also includes two fully disordered ligands (0.442(7): 0.558(7)) and 0.319(11): 0.681(11) occupancies. The occupancies are the same as observed previously within the standard uncertainties. As before, same distances and equal displacement parameter restraints and constraints (SHELXL SADI and EADP) were used to model these groups, while the pivot atoms (C14/14A and C24/24A) were split, but required to occupy the same position (EXYZ).

Crystal Data for $C_{16}H_{14}Br_2ClCuN_5O_6$ (M = 631.13 g/mol): monoclinic, space group $P2_1/c$ (no. 14), a = 21.4129(7) Å, b = 6.8466(2) Å, c = 16.6158(6) Å, β = 99.172(3)°, V = 2404.83(14) Å^3, Z = 4, T = 120.01 (10) K, μ(MoKα) = 4.382 mm^{-1}, $Dcalc$ = 1.743 g/cm^3, 14764 reflections measured (6.616° ≤ 2q ≤ 51.362°), 4577 unique (3895 with I > 2σ(I); R_{int} = 0.0347, R_{sigma} = 0.0359) which were used in all calculations. The final R_1 was 0.0469 (I > 2σ(I)) and wR_2 was 0.0961 (all data).

Table S1 Crystal data and structure refinement for **1** (with solvent mask) and **1-nm** (with disordered perchlorate ion; nm = no mask).

Cmpd/refinement	1	1-nm
Empirical formula	$C_{16}H_{14}Br_2ClCuN_5O_6$	$C_{16}H_{14}Br_2Cl_2CuN_5O_{10}$
Formula weight	631.13	730.58
Temperature /K	120.01(10)	
Crystal system	monoclinic	
Space group	$P2_1/c$	
a /Å	21.4129(7)	
b /Å	6.8466(2)	
c /Å	16.6158(6)	
α /°	90	
β /°	99.172(3)	
γ /°	90	
Volume /Å^3	2404.83(14)	
Z	4	
ρ_{calc} /g cm^{-3}	1.743	2.018
μ /mm^{-1}	4.382	4.516
F(000)	1236.0	1432.0
Crystal size /mm^3	0.19 × 0.158 × 0.06	
Radiation	MoKα (λ = 0.71073)	
2Θ range for data collection /°	6.616 to 51.362	
Index ranges	-26 ≤ h ≤ 25, -6 ≤ k ≤ 8, -16 ≤ l ≤ 20	
Reflections collected	14764	
Independent reflections	4577 [R_{int} = 0.0347, R_{sigma} = 0.0359]	
Data/restraints/parameters	4577/72/258	4577/202/334
Goodness-of-fit on F^2	1.127	1.096
Final R indexes [I>=2σ (I)]	R_1 = 0.0469 wR_2 = 0.0927	R_1 = 0.0634 wR_2 = 0.1424
Final R indexes [all data]	R_1 = 0.0565 wR_2 = 0.0961	R_1 = 0.0739 wR_2 = 0.1479
Largest diff. peak/hole / e Å^{-3}	0.77/-0.69	1.65/-1.36

Section III. Theory

Section III.1. Evaluation of J_{AB} magnetic interactions

We will now discuss the way the magnetic interaction J_{AB} between two A and B spin carriers will be computed for pyrazine-derivative compound **2**. Our First-Principles Bottom-Up FPBU approach uses the well-known two-body Heisenberg-Dirac-van Vleck spin Hamiltonian (HDVV) in which the isotropic interaction between localized magnetic moments $\mathbf{S}_A$ and $\mathbf{S}_B$ is given by:

$$\hat{H} = -2\sum J_{AB}\,\hat{S}_A \cdot \hat{S}_B$$

(Equation SIII.1.1)

where the sum runs over all different pairs of spin centers.

Within this framework, the value of the corresponding J_{AB} magnetic couplings is obtained taking advantage of the broken symmetry BS approach to describe the spin polarized electronic solutions to represent different spin orderings.[1,2,3] According to the strong localization limit of the spin mapping,[4,5] the Ising model (Equation SIII.1.2) provides the suitable mapping to extract the value of the J_{AB} magnetic couplings between radicals from the energy differences of BS states with different spin arrangement.[6]

$$\hat{H} = -2\sum J_{AB}\,\hat{S}_A^z \cdot \hat{S}_B^z$$

(Equation SIII.1.2)

If the model used to evaluate J_{AB} is a pair of radicals, the value of the magnetic coupling will be given by:

$$\Delta E = E^S - E^T = 2J_{AB} = \frac{2(E^{S,BS} - E^T)}{1 + S_{ab}^2}$$

(Equation SIII.1.3)

where ΔE is the energy difference between open-shell singlet E^S and triplet E^T states, $E^{S,BS}$ is the energy of the open-shell singlet state approximated using that of the single-determinant broken-symmetry (BS) solution,[1,2] and S_{ab} is the overlap between *magnetic orbitals*. The most common choice is to use the singly occupied orbitals (SOMOs) of the two monomers. However, according to Desplanches et al.[7], in the case of dinuclear complexes with bridging ligands, we cannot split the molecule into two independent, chemically meaningful monomers, and the use of the BS orbitals of the whole dinuclear entity seems to be a more general approach. Here we have thus followed this idea, which in turn has been extended to a tetramer model. For instance, Cu(II) atoms in the tetramer 1 model are interacting either mediated by pyrazine ligands (through J(6.83) and J(6.84) couplings) or through-space (J(9.63) and J(9.71) magnetic interactions) (see Figure SIII.1.1a). Analysis of spin-carrying moieties in the four magnetic orbitals of tetramer 1 shows that the orbitals have the same symmetry (dz^2 for Cu^{2+} and p-orbitals for pyrazine ligands directly coordinated to Cu(II), as well as quite diffuse orbitals on the counterions due to being anions). It

thus follows that the overlap is not negligible, and $J_{AB} = (E^{S,BS} - E^T)/2$ (see values listed in Table SIII.3.1 in '**SI Section III.3**').
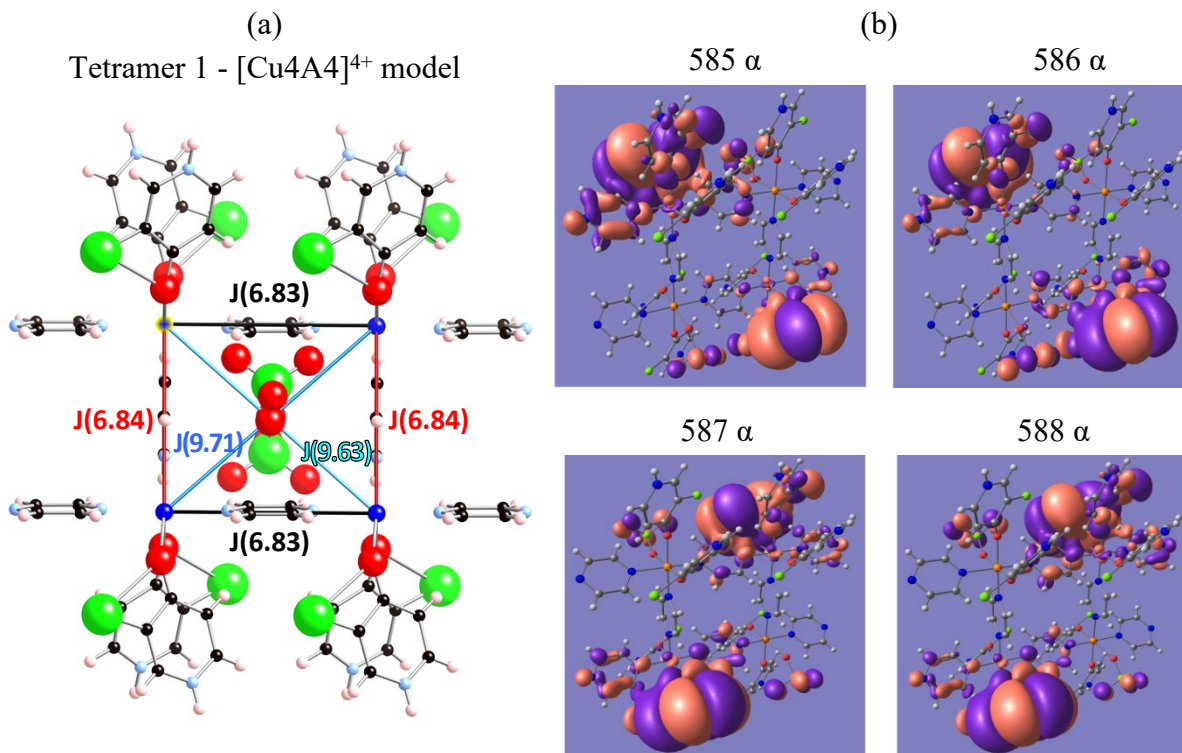
(a)

Tetramer 1 - [Cu4A4]$^{4+}$ model

(b)

585 α   586 α

587 α   588 α

Figure SIII.1.1. (a) [Cu4A4]$^{4+}$ model for Tetramer 1 of **2** crystal. (b) Four Singly Occupied Molecular Orbitals (SOMOs) corresponding to the quintet state of [Cu4A4]$^{4+}$ (tetramer 1) model.[8]

Note that the reported SOMOs in Figure SIII.1.1b belong to the quintet state of tetramer 1.[8] However, they could belong to the quintet state of any of the four studied tetramers. Let us stress here that the quintet orbitals have been used as the starting guess for energy calculations of all other low spin LS states and that the shape of them does not change (except for different combinations of α and β orbitals). Therefore, if the Cu atom shows dz^2-type SOMOs for the quintet, the same dz^2-type orbitals will persist in all other considered states, the most important difference among them being the different α and β combination. Since we computed several states with different multiplicities (e.g. for tetramer 1 we used 5 different models and computed a total of 25 states), and for each state there are 4 SOMOs, we here only present the quintet SOMO orbitals for succinctness (we let the reader to picture the shape of the SOMOs in the remaining states considered).

Referring the suitability of the molecular orbitals due to the volume of the orbitals located on Cu^{2+} (small) and ClO$_4^-$ (large), one must take into account that the spin density mainly lies in the Cu(II) atoms (Mulliken spin density ~0.65–0.70) and there is almost no spin density on the anions, except for the O atom semicoordinated to the Cu atoms (Mulliken spin density ~0.07, which is much

lower than the spin density on the Cu atoms). The SOMO pictures show big contributions of the anions because the Cu centers are formally cationic (the electronic density is more contracted) and the perchlorate ClO_4^- ligands are anions (with diffuse electronic density). Therefore, we are certain we are evaluating the coupling between the Cu(II) centers.

(a) Cu-based monomer without perchlorate counterions (dx^2-y^2 symmetry, see Cu)

(b) Cu-based monomer fully coordinated to pyrazine and ClO_4^- (dz^2 symmetry, see Cu)
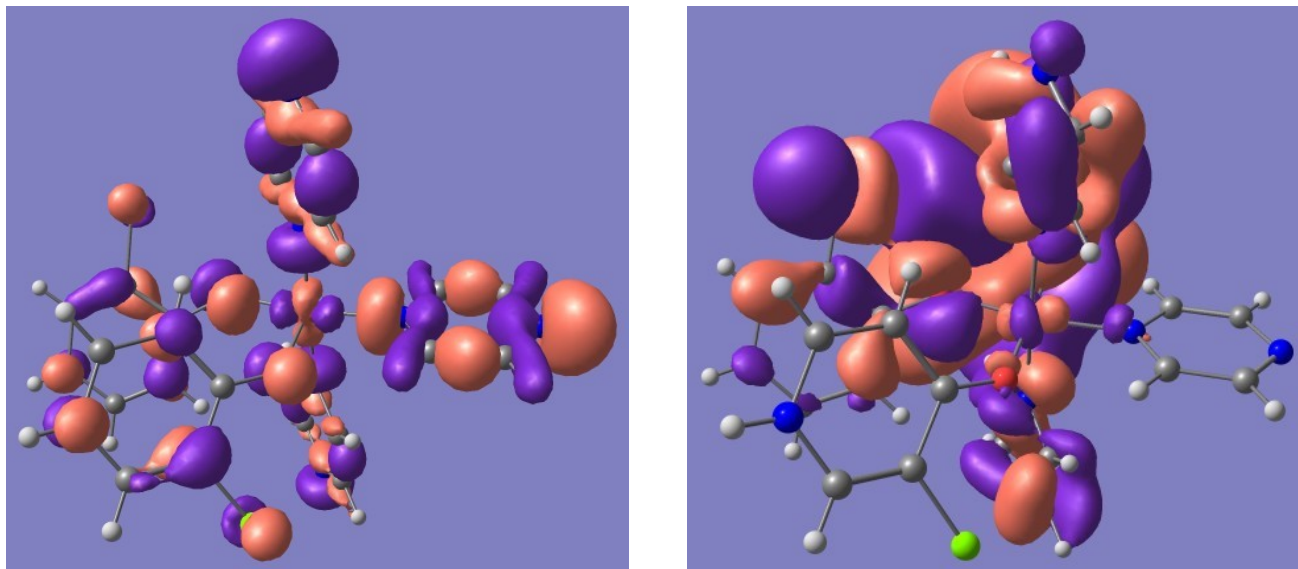

Figure SIII.1.2. SOMO corresponding to monomer (a) excluding and (b) including perchlorate ligands semicoordinated to the Cu(II)-moiety. Note that the symmetry of the atomic orbital of Cu(II) changes from (a) dx^2-y^2 when ClO_4^- ligands are not explicitly included to (b) dz^2 when taken into account.

In fact, regarding the role of the counterions on the J_{AB} values, previous experience on this family of compounds prompted us to study the impact of either the presence or the absence of perchlorate counterions prior to decide the size of the cluster model to be used to calculate all J_{AB} interactions. Our results showed that the orientation of the Cu orbitals changes substantially if coordinated perchlorate counterions are not included (see Figure SIII.1.2). Comparison shows that the dz^2 orbital localized on the Cu-atom when Cu is coordinated to pyrazine and perchlorate translates into a dx^2-y^2 orbital when Cu is only coordinated to pyrazine ligands. From this data, we concluded it was necessary to include all counterions directly coordinated to the Cu(II) atom and a tetramer cluster model was used to evaluate the value of all J_{AB} magnetic couplings.

Regarding the tetramer model used to evaluate the J_{AB} magnetic interaction between any two Cu-moieties, we have to calculate the energy of different spin arrangements, such as the high spin quintet state (Q) and some lower spin triplet (T) and singlet (S) states.[8] Considering the energies of these spin arrangements, it is then possible to devise relationships between these energies and the corresponding J_{AB} interactions involved in the aforementioned spin arrangements.

For instance, tetramer 1 involves 4 different magnetic couplings that have to be evaluated (see Figure SIII.1.3a). Therefore, 5 different spin states are required to calculate 4 J_{AB}'s. Figure SIII.1.3b schematically represents these 5 distinct spin arrangements along with the energy-J_{AB} relationships

(a) Tetramer 1	(b) Cu4 model
J(6.83), J(6.84), J(9.71), J(9.63), J(6.84), J(6.83)	Cu Cu ↑↑ ↓↑ ↑↓ ↓↑ ↓↓ Cu Cu ↑↑ ↑↑ ↑↑ ↑↓ ↑↑ Q T1 T2 S1 S2 T1 - Q = -5.257 = J(6.83) + J(6.84) + J(9.63) [1] T2 - Q = -5.257 = J(6.83) + J(6.84) + J(9.71) [2] S1 - Q = -10.502 = 2 J(6.83) + 2 J(6.84) S2 - Q = -4.828 = 2 J(6.83) + J(9.63) + J(9.71) Comparing [1] and [2], J(9.63) = J(9.71) = J(9) Result: J(6.83) = -2.41 cm^{-1} J(6.84) = -2.84 cm^{-1} J(9) = -0.01 cm^{-1}

Figure SIII.1.2. (a) J_{AB} magnetic couplings involved in the tetramer 1 cluster. (b) Relationships between energies and J_{AB}'s using the Cu4 model for tetramer 1 (see SI Section SIII.3 for discussion on models and Table SIII.3.1 for energies). Note Q, T# and S# stand for quintet, triplet, and singlet states, respectively.[8] Spin arrangement of high spin HS and low spin LS states is schematically given. All energies have been calculated at UB3LYP/6-31+G(d) level.

we have used to extract the values of J_{AB} interactions using the simplest Cu4 model for tetramer 1 (see SI Section III.3 for discussion on Cu4 model). Note that the same procedure has been followed using all remaining models for the 4 tetramers described in SI Section III.3. See Figure SIII.1.3 for the energy-J_{AB} relationships used for tetramers 2-4 to obtain the corresponding magnetic couplings using also the simplest Cu4 model.

Cu4 model	ΔE(LS# - HS)	Results
(a) tetramer2		
Cu Cu ↑ ↑ Cu Cu ↑ ↑ Q ↑ ↑ ↓ ↑ ↓ ↑	T1 - Q = -2.601 = J(6.83) + 2J(7.8) S1 - Q = -5.245 = 2J(6.83) + J(7.8) S2 - Q = -5.245 = 2J(6.83) + 2J(7.8)	**Considering states** **T1 and S1**: J(6.83) = -2.63 cm^{-1}, J(7.8) = 0.02 cm^{-1} **T1 and S2**: J(6.83) = -2.64 cm^{-1}, J(7.8) = 0.02 cm^{-1} **S1 and S2**: J(6.83) = -5.25 cm^{-1},
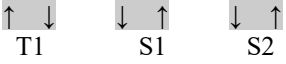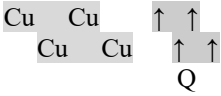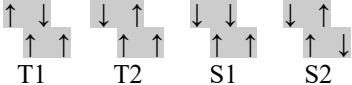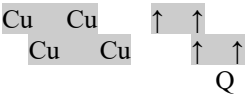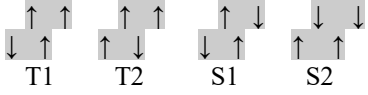
↑ ↓ ↓ ↑ ↓ ↑	$J(7.8) = 0.00$ cm^{-1}
T1 S1 S2	**Averaging the 3 sets of solutions** $J(6.83) = -2.63$ cm^{-1}, $J(7.8) = 0.02$ cm^{-1}

(b) tetramer3

Cu Cu ↑ ↑ Cu Cu ↑ ↑ Q	T1 - Q = -3.138 = J(6.84) + J(7.8) 　　　　　　　　 + J(8.94) T2 - Q = -3.149 = J(6.84) + J(8.94) S1 - Q = -6.277 = 2 J(6.84) + J(7.8) S2 - Q = -6.277 = 2 J(6.84) + J(8.90) 　　　　　　　　 + J(8.94)	J(6.84) = -3.15 cm^{-1} , J(7.8) = 0.01 cm^{-1} , J(8.90) = 0.02 cm^{-1} , J(8.94) = -0.00 cm^{-1}
↑ ↓ ↓ ↑ ↓ ↓ ↓ ↑ ↑ ↑ ↑ ↑ ↑ ↑ ↑ ↓ T1 T2 S1 S2		

(c) tetramer4

Cu Cu ↑ ↑ Cu Cu ↑ ↑ 　　　　　Q	T1 - Q = -0.011 = J(7.8) + J(8.94) T2 - Q = -2.787 = J(6.84) + J(7.8) 　　　　　　　　 + J(8.94) S1 - Q = -0.033 = 2J(7.8) + 2J(8.94) S2 - Q = -2.787 = J(6.84) + 2 J(7.8)	**Considering states** **T1, T2 and S2**: J(6.84) = -2.77 cm^{-1}, J(7.8) = -0.01 cm^{-1}, J(8.94) = -0.01 cm^{-1} **T2, S1 and S2**: J(6.84) = -2.79 cm^{-1}, J(7.8) = -0.02 cm^{-1}, J(8.94) = -0.02 cm^{-1} **Averaging the 2 sets of solutions** J(6.84) = -2.78 cm^{-1}, J(7.8) = -0.01 cm^{-1}, J(8.94) = -0.01 cm^{-1}
↑ ↑ ↑ ↑ ↑ ↓ ↓ ↓ ↓ ↑ ↑ ↓ ↓ ↑ ↑ ↑ T1 T2 S1 S2		

Figure SIII.1.3. Spin arrangement of high spin HS and low spin LS states is schematically represented along with relationships between energies and J_{AB}'s using the Cu4 model for (a) tetramer 2, (b) tetramer 3 and (c) tetramer 4 clusters (see SI Section SIII.3 for discussion on models and Table SIII.3.1 for energies). Note Q, T# and S# stand for quintet, triplet, and singlet states, respectively.[8] All energies have been calculated at UB3LYP/6-31+G(d) level.

———————————

1. L. Noodleman, *J. Chem. Phys.* **1981**, 74, 5737–5743

2. L. Noodleman and E. R. Davidson, *Chem. Phys.* **1986**, 109, 131–143

3. R. Caballol, O. Castell, F. Illas, I. de P. R. Moreira, and J. P. Malrieu, *J. Phys. Chem. A*, **1997**, 101, 7860–7866

4. I. de P. R. Moreira, F. Illas *Phys. Chem. Chem. Phys*., **2006**, *8*, 1645–1659.

5. I. de P. R. Moreira, C. J. Calzado, J-P. Malrieu, F. Illas, *New J. Phys.* **2007**, *9*, 369.

6. P. Rivero, I. de P. R. Moreira, F. Illas *J. Phys.: Conf. Series* **2008**, *117*, 012025.

7. C. Desplanches, E. Ruiz, A. Rodríguez-Fortea, S. Alvarez, *J. Am. Chem. Soc.* **2002**, *124*, 5197-5205

8. Note that the broken symmetry (BS) states are only eigenfunctions of $\hat{S}_z$. Here we use the nomenclature Quintet, Triplet, and Singlet to make the discussion easier for a non-quantum chemist. We actually refer to states with eigenvalues $S_z=2$ as Quintet, $S_z=1$ as Triplet and $S_z=0$ as Singlet, although *stricto sensu* these states cannot be named after their alleged $\hat{S}^2$ eigenvalues.

Section III.2. About the size of the basis set used to compute J_{AB} interactions

In order to evaluate the J_{AB} magnetic coupling between Cu-moieties, basis sets of different size were tested. The toy system used was the pair of pyrazine-bridged radicals whose Cu⋯Cu distance is shortest, i.e. 6.833 Å (see Figure SIII.2.1). We chose precisely this pair of Cu-moieties because they are bridged by pyrazines and, thus, its J_{AB} magnetic coupling value is expected to be similar to that obtained using a tetramer model. However, in case of through-space J_{AB} interactions, the tetramer model is mandatory. With the aim of assessing the influence of the basis set on the calculated value of the magnetic coupling, we tried double- and triple-zeta basis sets with and without diffuse and polarization functions, namely, 6-31G, 6-31+G(d), and 6-311+G(d,p). Our results show that the energy difference between triplet and broken-symmetry singlet states depends on polarization and diffuse functions, but it is not very sensitive to double- and triplet-zeta splitting (see Table SIII.2.1). Comparison of SOMOs (see Figure SIII.2.2) indicates that the orbitals belonging to the perchlorate anion become larger as more diffuse and polarization functions are included in the basis set, which was to be expected. Besides it is also clearly observed that the orbitals located on the pyrazine-bridge and the Cu atoms do not change size. We must stress that the orbitals of ClO_4^- anions are very bulky due to the fact that anions have an intrinsic diffuse electronic density, whereas the electronic density is more contracted in Cu centers because they formally are cationic.

Therefore, taking into consideration the size of the tetramer model (*ca.* 200 atoms), we have chosen to carry out all energy calculations using the 6-31+G(d) basis set which is medium size but accurate to obtain J_{AB} couplings. Note that for discussion purposes we will compare J_{AB} results obtained using 6-31G and 6-31+G(d) basis sets in next '**SI Section III.3**'.
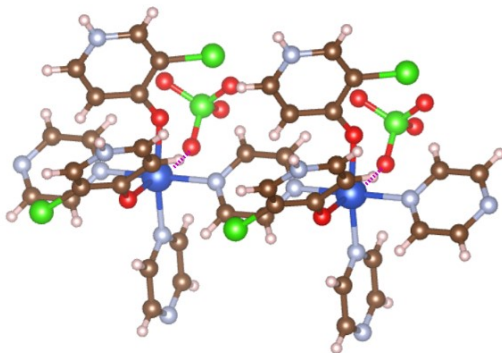

Figure SIII.2.1. Toy system used to calculate the J_{AB} interaction using different basis sets for the pair of pyrazine-bridged radicals whose Cu⋯Cu distance is shortest, i.e. 6.833 Å.
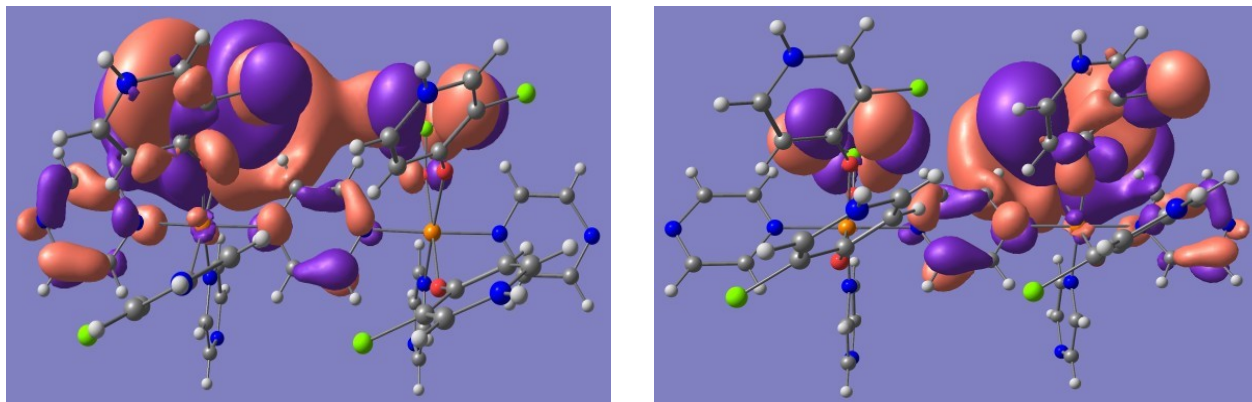
Table SIII.2.1. Calculated J(6.83) magnetic coupling (in cm^{-1}) using the dimer model shown in Figure SIII.2.1, which considers 2 Cu-moieties bridged by one pyrazine ligand. All energies have been computed at the UB3LYP level.

basis set	6-31G	6-31+G(d)	6-311+G(d,p)
J(6.83) / cm^{-1}	-3.0	-4.0	-3.8

(a) 6-31G basis set
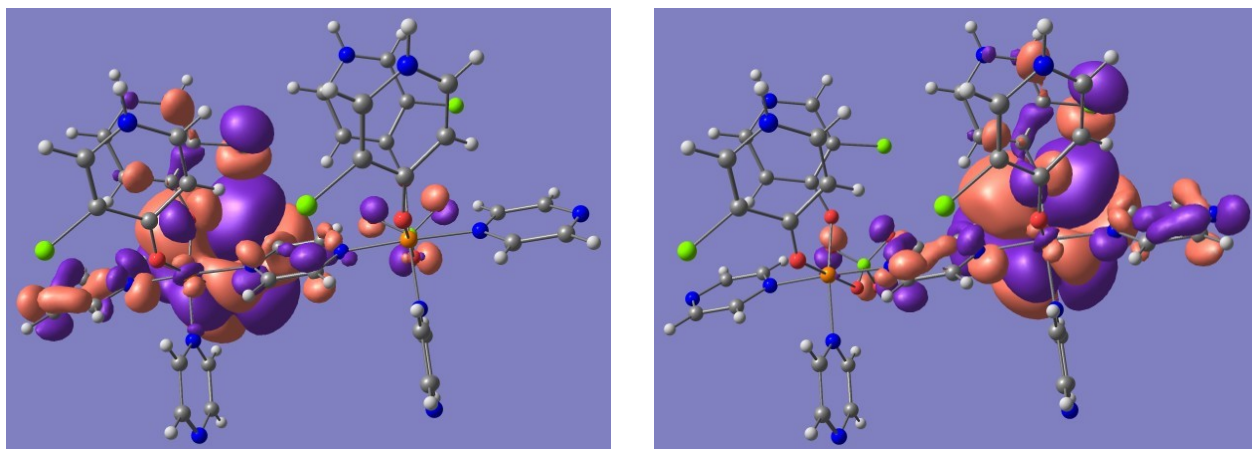
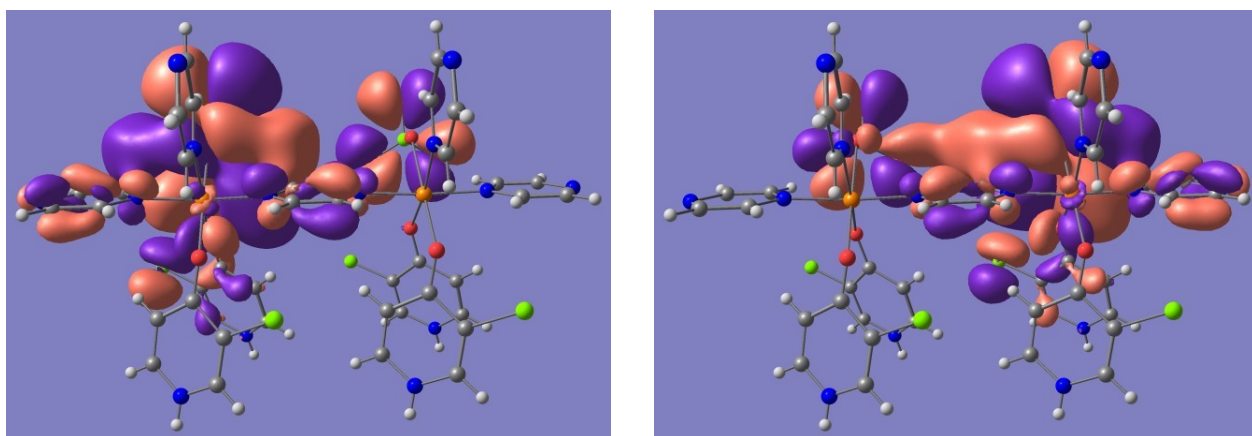

(b) 6-31+G(d) basis set

(c) 6-311+G(d,p) basis set

Figure SIII.2.2. Singly occupied molecular orbitals SOMOs calculated at UB3LYP level using (a) 6-31G, (b) 6-31+G(d), and (c) 6-311+G(d,p) basis sets.

Section III.3. About the accuracy of the different tetramer models used to compute J_{AB} interactions

In order to evaluate the J_{AB} magnetic coupling between Cu-moieties, four families of tetramer models were selected (see Figures SIII.3.1-4). Tetramers 1 and 2 were chosen to evaluate J_{AB} between two intra-ladder spin carriers at 6.833Å (black, along the *b*-axis). Tetramer 1 connects two pairs of spin carriers at 6.833 Å by shortest interdimer contacts, 6.842 Å (red, Figure SIII.3.1), and tetramer 2 connects two pairs of spin carriers by the next shortest interdimer contacts, 7.823 Å (green, Figure SIII.3.2). Tetramers 3 and 4 are used to assess pairs of spin carriers connected along the *c*-axis at 8.902 and 8.942 Å (i.e. inter-ladder couplings, Figures SIII.3.3-4). Notice that magnetic interactions between spin carriers at 6.833 and 6.842 Å are mediated by a pyrazine ligand, while all the others are through-space magnetic interactions.

Let us remark that each tetramer model has been chosen paying special attention to which weak interactions have to be accounted in order to describe adequately the environment of each spin carrying Cu center: it is not only the number of perchlorate anions but also their coordination and interaction with the bridging pyrazines, which is crucial in order to compute the value of J_{AB} couplings between Cu-moieties. Therefore, in a second step, the role of the counterions was taken into account and several clusters have been built by choosing some of the perchlorate anions in the vicinity of the Cu(II) ions. Although for the four tetramers the same number of counterions have been used (0, 2, 4 and 6), their relative positions with respect the Cu centers and, thus, their role, are different in each case. It is possible to distinguish between semi-coordinated anions (to the Cu ions) and hydrogen bonding counterions. In most of the cases these two roles are shared by the same ClO_4^- molecule, so the analysis of the computed values of J_{AB} magnetic interactions (shown in Table SIII.3.1) is not straightforward.

Specifically, in the $[Cu4A2]^{6+}$ tetramer 1 model, the two ClO_4^- anions lie on top and bottom positions in the center of the Cu4 plane (see Figure SIII.3.1a). The shortest Cu···O distances vary between 4.5 and 4.9 Å. These anions also display short interactions (about 2.5 Å) with some of the H of the pyrazine ligands (see dashed lines in Figure SIII.3.1a). The $[Cu4A4]^{4+}$ tetramer1 model is not built by adding two ClO_4^- anions (A) to the smaller $[Cu4A2]^{6+}$ tetramer1 model but consists of the Cu4pz framework with the four corresponding semi-coordinated ClO_4^- anions (Cu···Cl distance at 2.65Å). Note that each anion fills an octahedral coordination site of a given Cu center (dashed purple lines in Figure SIII.3.1b). Hydrogen bonds are also created (see dashed blue lines as shown in Figure SIII.3.1b), but only some of them have a good orientation to interact with pyrazine ligands (see bridging pyrazine along the *b*-axis with O···H distance 2.30 Å, the orientation is not the best and the pyrazine that connects the Cu ions at 6.84 Å with O···H distance at 2.32 Å). Similarly, the $[Cu4A6]^{2+}$ cluster model includes all the counterions mentioned before, i.e. the six ClO_4^- anions of both $[Cu4A2]^{2+}$ and $[Cu4A4]^{2+}$ models (dashed blue lines for hydrogen bonds and purple dashed lines for semi-coordinated anions in Figure SIII.3.1c). Finally, two perchlorate anions can be added to the $[Cu4A6]^{2+}$ cluster to form the neutral (charge 0) $[Cu4A8]$ aggregate, resulting in new hydrogen bonds (see Figure SIII.3.1d, dashed blue lines).

(a) [Cu4A2]$^{6+}$ tetramer1 model

(b) [Cu4A4]$^{4+}$ tetramer1 model

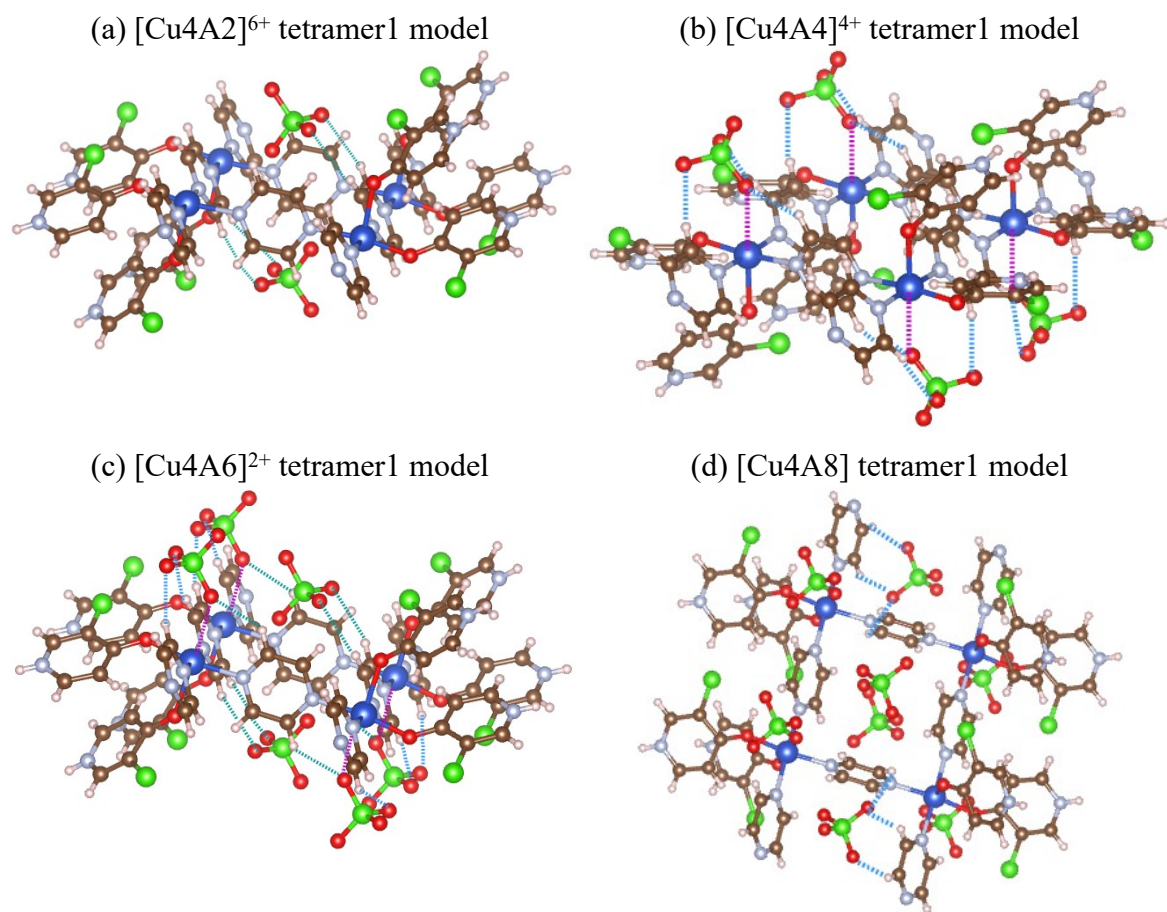(c) [Cu4A6]$^{2+}$ tetramer1 model

(d) [Cu4A8] tetramer1 model

Figure SIII.3.1. Different copper-pyrazine arrangements considered to assess the value of J_{AB} magnetic interactions in the tetramer 1 cluster model by accounting for (a) two, (b) four, (c) six, and (d) eight ClO$_4^-$ counterions.
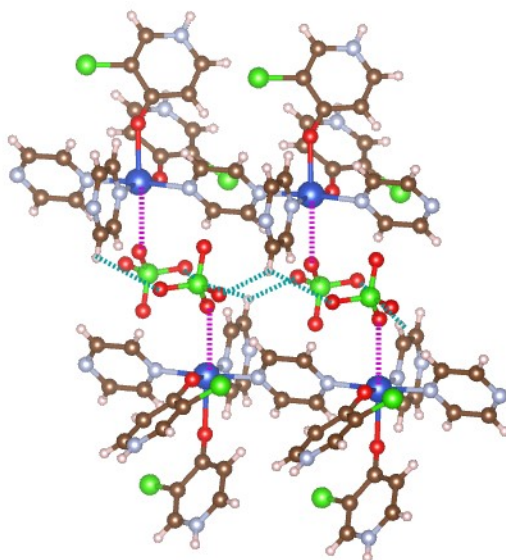
Figure SIII.3.2. [Cu4A4]$^{4+}$ cluster for the tetramer 2 model

Regarding tetramer 2, a $[Cu4A4]^{4+}$ cluster includes all the corresponding ClO_4^- anions semi-coordinated to the Cu ions (purple dashed lines in Figure SIII.3.2). In addition, these ClO_4^- anions also interact with nearby pyrazine ligands belonging to other Cu centers by means of hydrogen bonds (O···H distances 2.64-2.65 Å, blue dashed lines in Figure SIII.3.2). No more models for this tetramer have been considered, since nearest counterions (not the already included in the model) lie far from the Cu ions and their consideration would not make chemical sense.
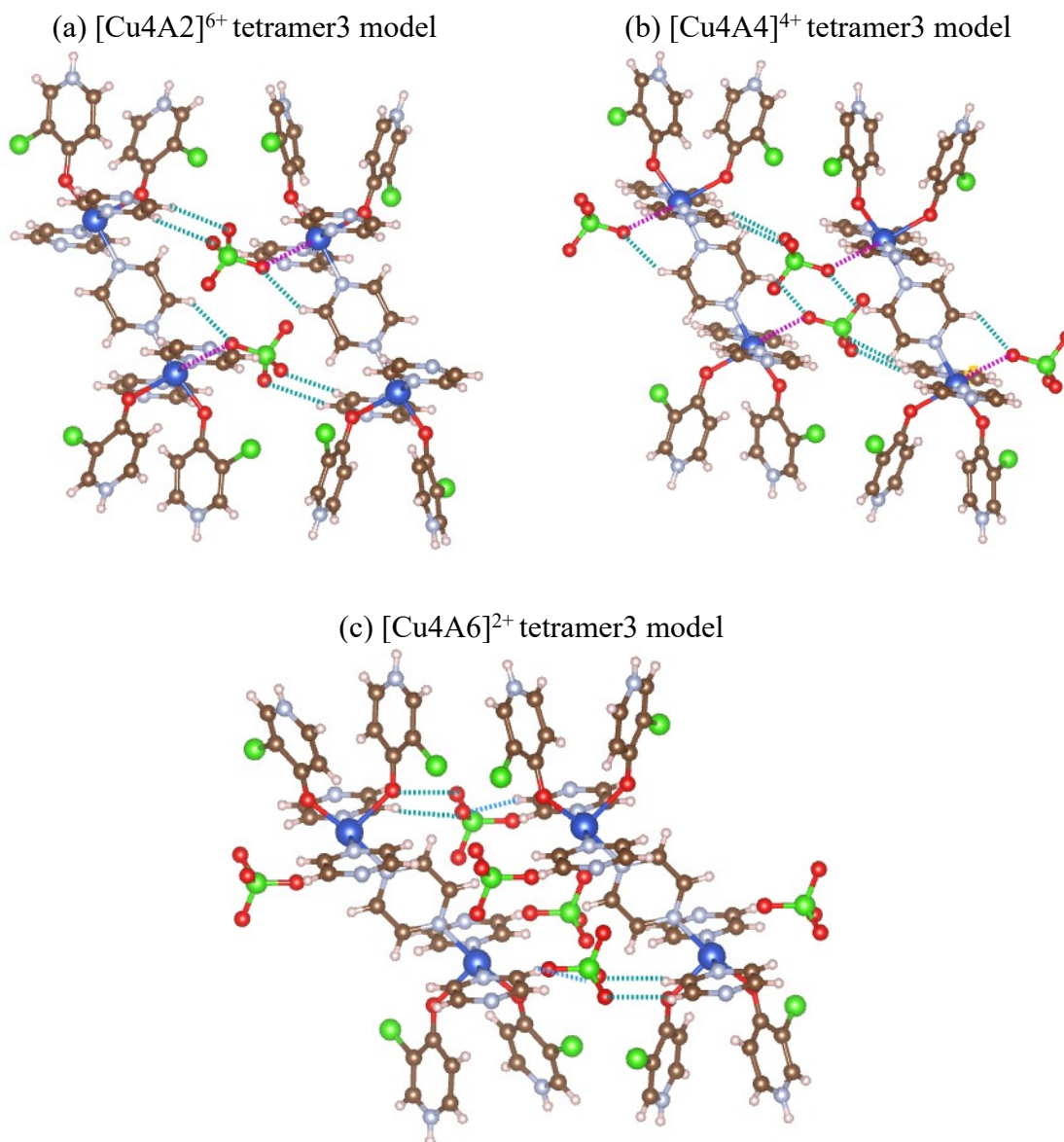
(a) $[Cu4A2]^{6+}$ tetramer3 model

(b) $[Cu4A4]^{4+}$ tetramer3 model

(c) $[Cu4A6]^{2+}$ tetramer3 model

Figure SIII.3.3. Different copper-pyrazine arrangements considered to assess the value of J_{AB} magnetic interactions in the tetramer 3 cluster model by accounting for (a) two, (b) four, and (c) six, ClO_4^- counterions. Note that in (c) only the hydrogen bonds created by adding two perchlorate anions to the $[Cu4A4]^{4+}$ tetramer are represented in blue dashed lines.

With respect to tetramer 3, in the [Cu4A2]$^{6+}$ model the two anions lie in the middle of two different Cu-pz-Cu units. They are both semi-coordinated to one Cu ion each (purple dashed lines in Figure SIII.3.3a) and at the same time establish two hydrogen bonds with pyrazines belonging to the close Cu-pz-Cu frames (blue dashed lines in Figure SIII.3.3a). The [Cu4A4]$^{4+}$ tetramer3 model was built by adding two anions to saturate the Cu octahedral coordination. These two ClO$_4^-$ anions are external (purple dashed lines in Figure SIII.3.3b) to the cluster and only one hydrogen bond is created by each new anion. In order to construct the [Cu4A6]$^{2+}$ aggregate, two new nearby ClO$_4^-$ anions are added to the [Cu4A4]$^{4+}$ tetramer3 model that interact with other pyrazine ligands coordinated to the same Cu ion via hydrogen bonds (O···H distances about 2.30 Å, blue dashed lines in Figure SIII.3.3c). However, they are not coordinated to any Cu ion in the model. They are equivalent to the two ClO$_4^-$ anions in the first [Cu4A2]$^{2+}$ tetramer3 model, but they are not coordinated to any Cu ion.

(a) [Cu4A2]$^{6+}$ tetramer4 model   (b) [Cu4A4]$^{4+}$ tetramer4 model
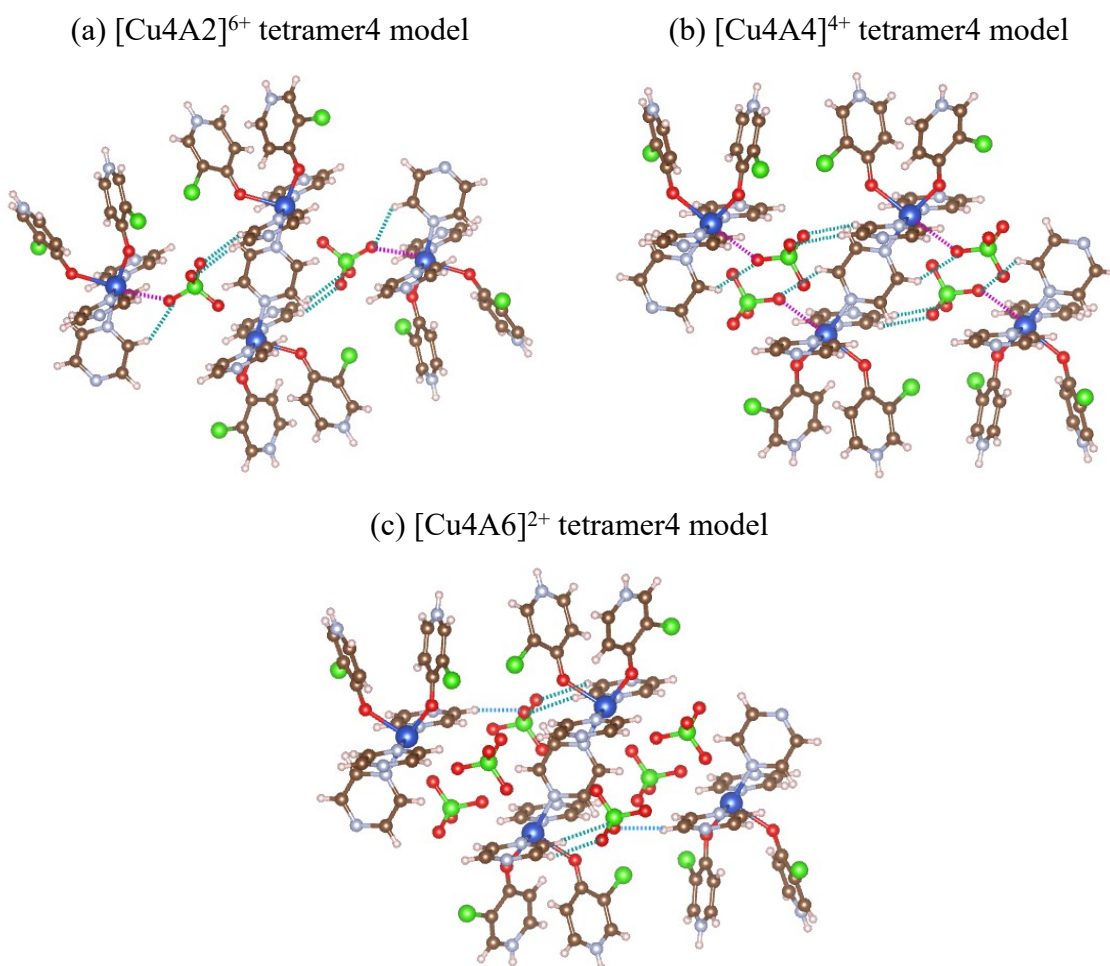

(c) [Cu4A6]$^{2+}$ tetramer4 model

Figure SIII.3.4. Different copper-pyrazine arrangements considered to assess the value of J_{AB} magnetic interactions in the tetramer 4 cluster model by accounting for (a) two, (b) four, and (c) six, ClO$_4^-$ counterions. Note that in (c) only the hydrogen bonds created by adding two perchlorate anions to the [Cu4A4]$^{4+}$ tetramer are represented in blue dashed lines

Table SIII.3.1. Calculated J_{AB} magnetic coupling (in cm^{-1}) using different models for tetramers 1, 2, 3 and 4 which consider 4 Cu-moieties, the pyrazine ligands involved in the Cu skeleton, and a given number of ClO$_4^-$ counterions (see above discussion, and Figures SIII.3.1-SIII.3.4). Name code: Cu4 stands for no ClO$_4^-$ counterions; Cu4A# stands for the copper-pyrazine skeleton and # number of counterions (note # = 2, 4, 6 and 8). All energies have been computed at the UB3LYP level.

model	tetramer1					tetramer2		tetramer3				tetramer4			
	Cu4	Cu4A2	Cu4A4	Cu4A6	Cu4A8	Cu4	Cu4A4	Cu4	Cu4A2	Cu4A4	Cu4A6	Cu4	Cu4A2	Cu4A4	Cu4A6
6-31G															
J(6.83)	-2.02	-3.60	-2.92	-5.03	-4.17	-2.31	-3.00	-	-	-	-	-	-	-	-
J(6.84)	-2.13	-4.08	-3.12	-4.81	-6.65	-	-	-2.48	-3.17	-3.56	-4.39	-2.27	<|0.05|	-3.76	-5.94
J(7.82)	-	-	-	-	-	0.07	<|0.05|	<|0.05|	0.0	<|0.05|	<|0.05|	<|0.05|	0.0	<|0.05|	0.0
J(8.90)	-	-	-	-	-	-	-	<|0.05|	0.0	<|0.05|	0.0	-	-	-	-
J(8.94)	-	-	-	-	-	-	-	<|0.05|	0.0	<|0.05|	<|0.05|	<|0.05|	0.0	<|0.05|	0.0
"J9"	0.0	<|0.05|	<|0.05|	<|0.05|	0.0	-	-	-	-	-	-	-	-	-	
6-31+G(d)															
J(6.83)	-2.41	-4.88	-4.04	-6.96	-6.07	-2.63	-4.02	-	-	-	-	-	-	-	-
J(6.84)	-2.84	-5.66	-3.89	-7.02	-9.33	-	-	-3.15	-4.20	-4.73	-5.97	-2.78	-4.35	-5.04	-8.23
J(7.82)	-	-	-	-	-	<|0.05|	<|0.05|	<|0.05|	<|0.05|	<|0.05|	<|0.05|	<|0.05|	<|0.05|	<|0.05|	0.0
J(8.90)	-	-	-	-	-	-	-	<|0.05|	<|0.05|	<|0.05|	0.0	-	-	-	-
J(8.94)	-	-	-	-	-	-	-	<|0.05|	<|0.05|	<|0.05|	<|0.05|	<|0.05|	<|0.05|	<|0.05|	0.0
"J9"	<|0.05|	<|0.05|	<|0.05|	<|0.05|	<|0.05|	-	-	-	-	-	-	-	-	-	-

Finally, a [Cu4A2]$^{6+}$ tetramer4 model consists of four Cu centers with two semi-coordinated anions to one Cu ion each (purple dashed lines in Figure SIII.3.4a). At the same time, these two ClO$_4^-$ anions display hydrogen bonds with pyrazines (blue dashed lines in Figure SIII.3.4a). In the [Cu4A4]$^{4+}$ tetramer4 model, two ClO$_4^-$ anions are added in such a way that all the Cu centers are semi-coordinated to the ClO$_4^-$ anions (purple dashed line in Figure SIII.3.4b), although they form only one hydrogen bond each (blue dashed line in Figure SIII.3.4a). Finally, to construct the [Cu4A6]$^{2+}$ tetramer 4 aggregate, two ClO$_4^-$ anions are added to the [Cu4A4]$^{4+}$ tetramer4. They interact with other pyrazine ligands coordinated to the same Cu ion via hydrogen bonds (O$\cdots$H distances about 2.30 Å, blue dashed lines in Figure SIII.3.4c), but they are not coordinated to any Cu ion in the model, as occurred in [Cu4A6]$^{2+}$ for tetramer 3.

Concerning the J_{AB} calculated values shown in Table SIII.3.1, addition of counterions to the model increases the antiferromagnetic coupling in all the cases. The use of a large basis set such as 6-31+G(d), which includes both polarization and diffuse functions, is also important in order to properly describe all the weak interactions involved.
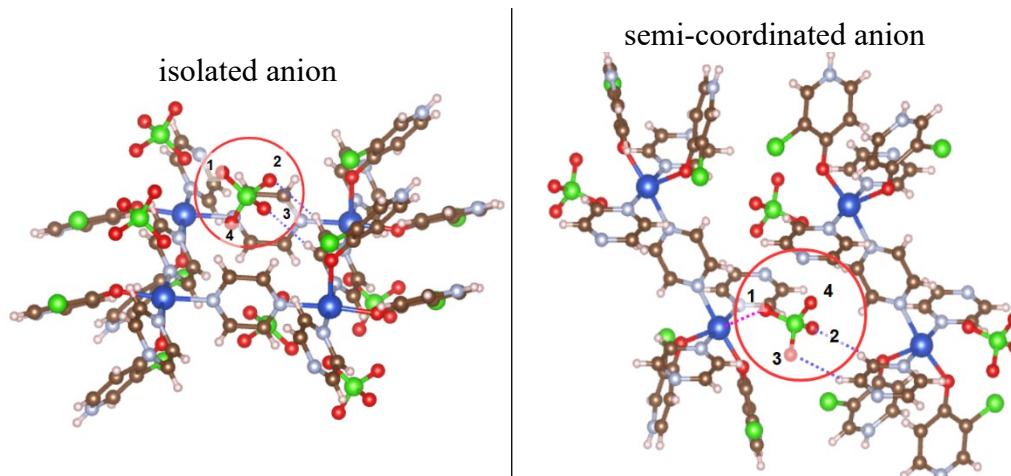
atom	Mulliken charge / Mulliken spin density	
1	-0.299911 / -0.000014	-0.447798 / -0.002296
2	-0.356944 / 0.000118	-0.112230 / -0.000517
3	-0.365440 / 0.000161	-0.155035 / -0.009967
4	-0.441568 / 0.000269	-0.228889 / -0.000019

Figure SIII.3.5. Mulliken charges and spin population for the tetramer 1 $[Cu2A6]^{2+}$ model (isolated anion) and tetramer 3 $[Cu2A6]^{2+}$ model (semi-coordinated anion) computed at the UB3LYP/6-31+G(d) level. There is a rotation between the images of the two models (this is why the numbering in the semi-coordinated anion image is not correlative).

Regarding the quality of the models, it is quite surprising that the *medium size* $[Cu4A4]^{4+}$ model reproduces better the experimental behavior than a larger one, such as $[Cu4A6]^{2+}$, which one would expect it would include more effects present in the crystal. In order to rationalize this fact, the analysis of the Mulliken charges and spin population of the anions depending on whether they are semi-coordinated or not to a Cu ion has been carried out. It shows that the interaction with the metal ion is crucial and, thus, it changes completely the charge and spin distribution of the perchlorate anion (see Figure SIII.3.5). On the one hand, the Mulliken charge of the O atoms involved in the hydrogen bonds (see oxygen atoms numbered 2, 3 in Figure SIII.3.5) is much larger when the anion is isolated (about -0.5) than when it is semi-coordinated (*ca.* -0.14). We can then conclude that, in $[Cu4A6]^{2+}$ models, the hydrogen bond interaction is overestimated when the anion is not coordinated to a Cu ion (as it happens in the solid). It has been further assessed that the O which coordinates to a Cu ion (number 1 in Figure SIII.3.5), has the largest negative charge (-0.45), but it becomes the lowest charge (-0.30) when the anion is isolated. It thus follows that the electrostatics of the semi-coordinated and the isolated anions are very different. Clearly the use of isolated anions in the model could induce errors when evaluating J_{AB} interactions in this compound. Concerning the spin density, the O atoms involved in hydrogen bonds do not have significant values both in the isolated and the semi-coordinated anion. However, when an O atom coordinates the Cu ion, it carries some spin density (-0.002571). Although it is a small value, it is

much larger than in the isolated anion (-0.000014). We can thus conclude that modeling the perchlorate anions without taking into account its semi-coordination leads to errors when computing the magnetic interaction between Cu-pz-moieties. Therefore, the [Cu4A4]$^{4+}$ tetramer 1 model, which has all the perchlorate anions semi-coordinated, should perform better than the [Cu4A6]$^{2+}$ or [Cu4A8] models, which include non-semi-coordinated anions, and nicely reproduce the experimental data. In this sense, values in Table SIII.3.1 for [Cu4A4]$^{4+}$ models that have semi-coordinated anions compare well. However, when isolated perchlorates are included, the J_{AB} values increase but cannot be used to simulate the magnetic response (as we will next show). This effect is very clear in all [Cu4A6]$^{2+}$ clusters and in the [Cu4A8] model. This conclusion is also extracted from the magnetic susceptibility simulations (see Figure SIII.4.1 in SI Theory Section III.4). In summary, one must make sure that the Cu coordination is accurately described in order to rely on the computed J_{AB} data. We refer to Table 8 in main text for J_{AB} most reliable values, and to Figure SIII.3.6 for final compilation of all [Cu4A4]$^{4+}$ models

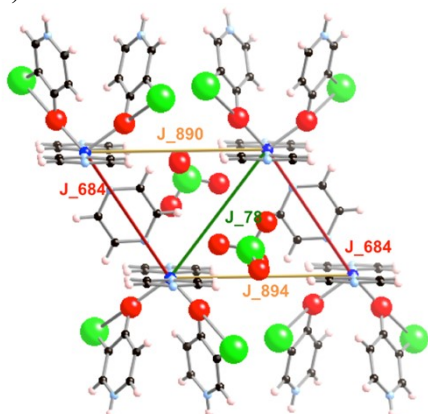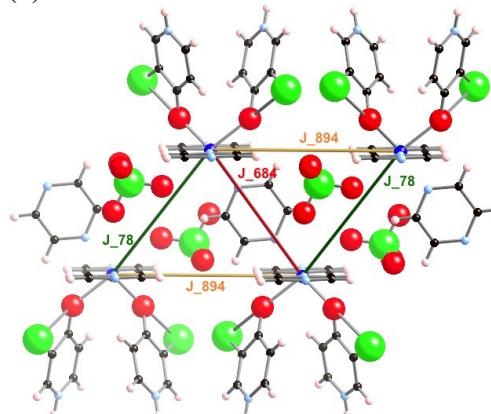(a) tetramer 1
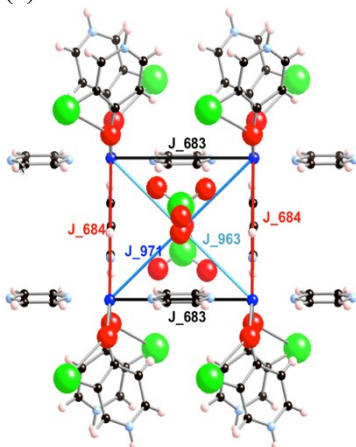
(b) tetramer 2
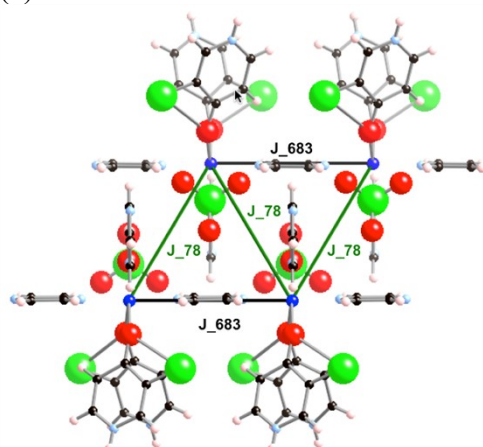
(c) tetramer 3

(d) tetramer 4

Figure SIII.3.6. Display of clusters [Cu4A4]$^{4+}$ models used to compute the J_{AB} magnetic interaction between pairs of Cu-moieties: (a) tetramer 1, (b) tetramer 2, (c) tetramer 3, and (d) tetramer 4. Color code: J_{AB} mediated by pyrazines: J_683 in black and J_684 in red ; and through-space J_{AB} interactions: J_78 in green, J_890 in orange, J_894 in brown, J_963 in cyan, and J_971 in blue. Note that # in J_# stands for the distance between Cu ions in angstroms (i.e. J_78 = J_{AB} for 7.8 Å Cu···Cu separation).

Section III.4. On the simulation of the magnetic response

The resulting magnetic susceptibility $\chi(T)$ data has been calculated using J_{AB} values extracted from the tetramer 1 Cu·pz-perchlorate clusters because it is the only model that explicitly includes the two meaningful magnetic interactions J(6.83) and J(6.84). Calculated $\chi(T)$ and $\chi T(T)$ data using the J_{AB} values obtained with the [Cu4A4]$^{4+}$ and [Cu4A6]$^{2+}$ models are shown in Figure SIII.4.1 (empty and full blue symbols, respectively). In all simulations the experimental g=2.14 value is used. Clearly the computed data using the J_{AB} values obtained from the [Cu4A4]$^{4+}$ model fit the experimental data nearly perfectly. Therefore, in the main text we will exclusively refer to results obtained with the use of the [Cu4A4]$^{4+}$ models since they not only reproduce the experimental data better, but also describe accurately the Cu-coordination within the crystal.
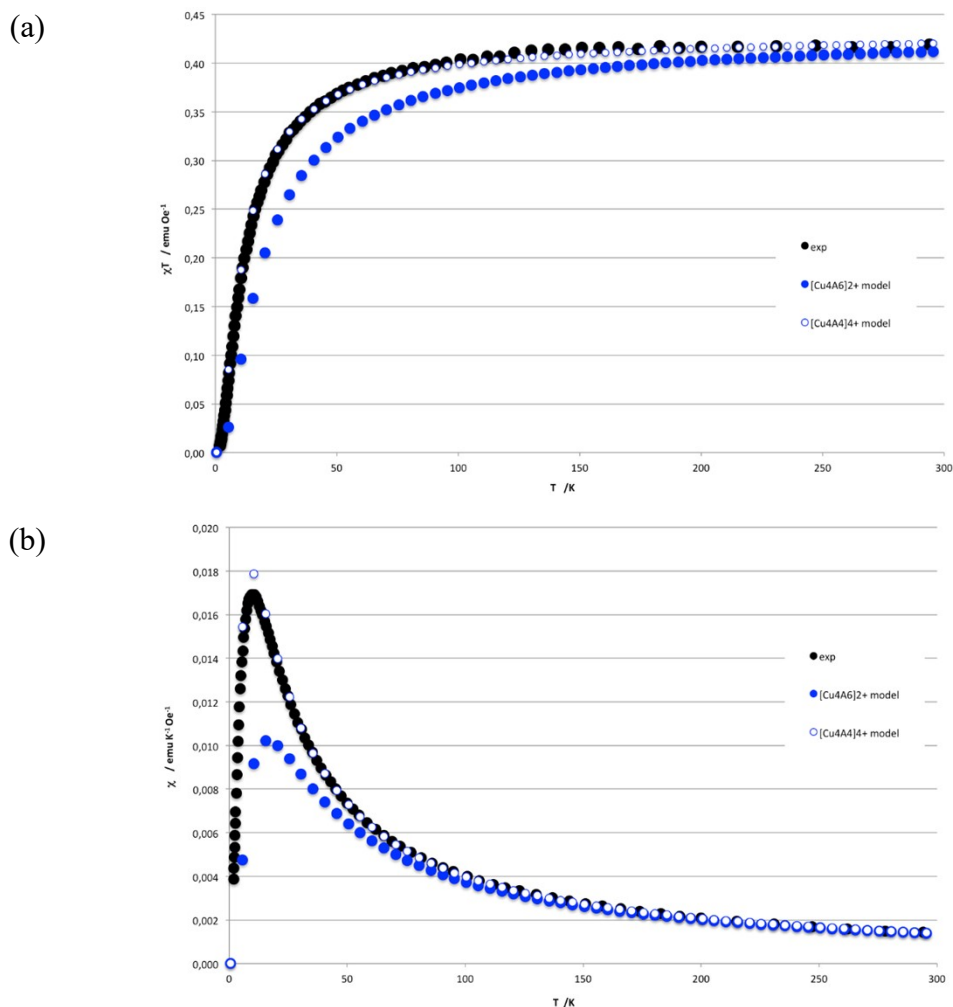

Figure SIII.4.1. Comparison between experimental (black circles) and calculated magnetic susceptibility (a) χT and (b) χ as a function of temperature using the [Cu4A4]$^{4+}$ (empty blue circles) and [Cu4A4]$^{4+}$ (full blue circles) models.
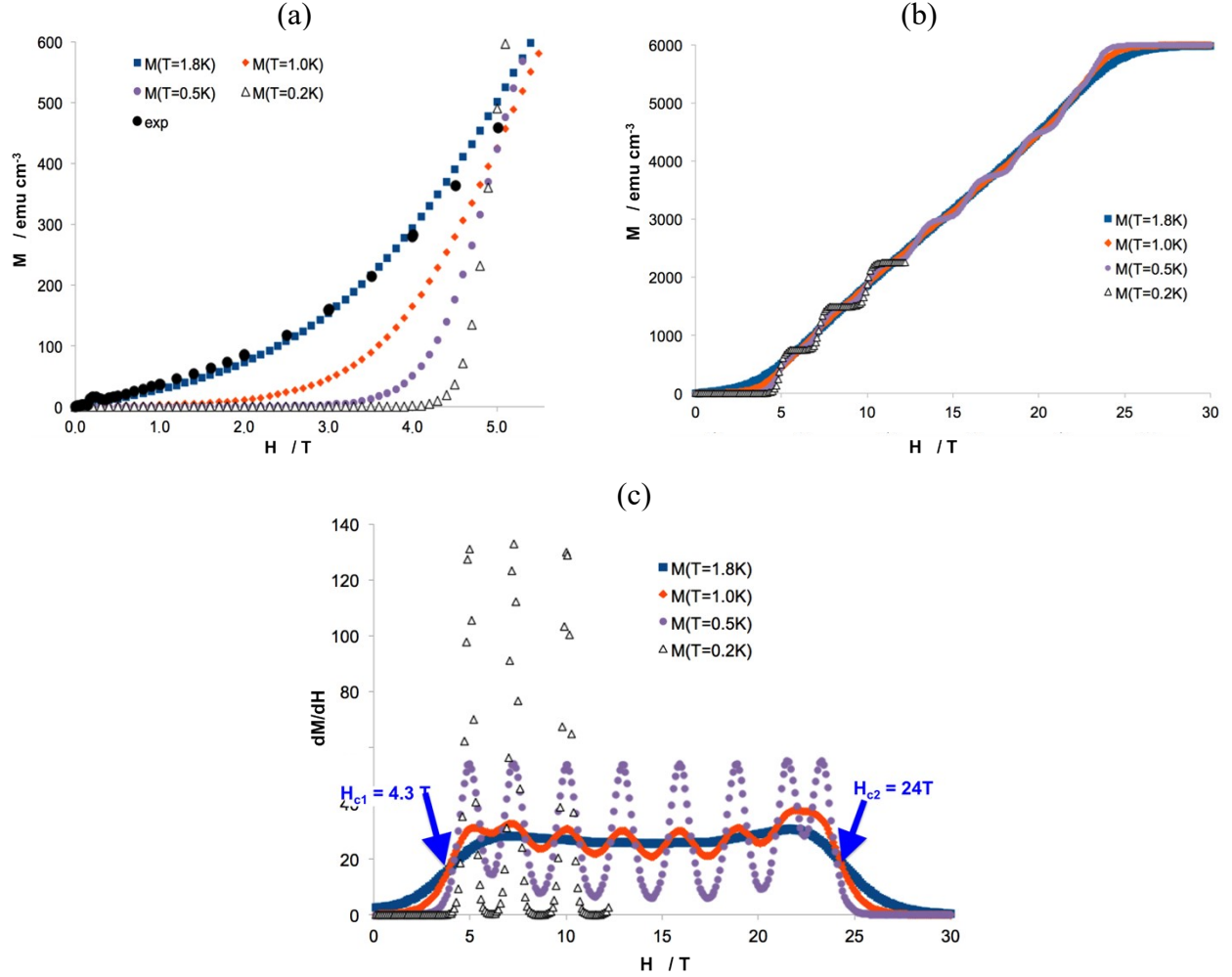
Figure SIII.4.2. Magnetization as a function of magnetic field at 1.8K, 1.0K, 0.5K and 0.2K in the range (a) to 5T, and (b) to saturation at *ca.* 20 T. (c) dM/dH as a function of magnetic field showing H_{c_1} and H_{c_2}.

The calculated magnetization to 5 T at 1.8K is also in agreement with the experimental available data at 1.8K (see Figure SIII.4.2a-b). Experimentally, at 1.8 K, **2** is still approaching a singlet ground state and, thus, the critical field H_{c_1} is not observable; lower temperature and higher field magnetization studies are necessary to experimentally observe and quantify H_{c_1} and H_{c_2}. Our simulations indicate that saturation is reached at $H_{c_2} \sim 24$ T (see inflection point in Figure SIII.4.2c for a better realization). This result is in line with the estimates from both mean-field approximation (24T) and using the average g-factor from susceptibility measurements (*vide infra*) (28T). As for H_{c_1}, our simulations below 1.8K give an estimate of ca. 4.3T (see Figure SIII.4.2c) and suggest a quantum dominated magnetic spectrum (see Figure SIII.4.2b). Note that both H_{c_1}

and H_{c_2} have been estimated from averaging the values of the magnetic field at which dM/dH became an inflection point at 1.0, 0.5 and 0.2 K (i.e. at temperatures well below 1.8 K).
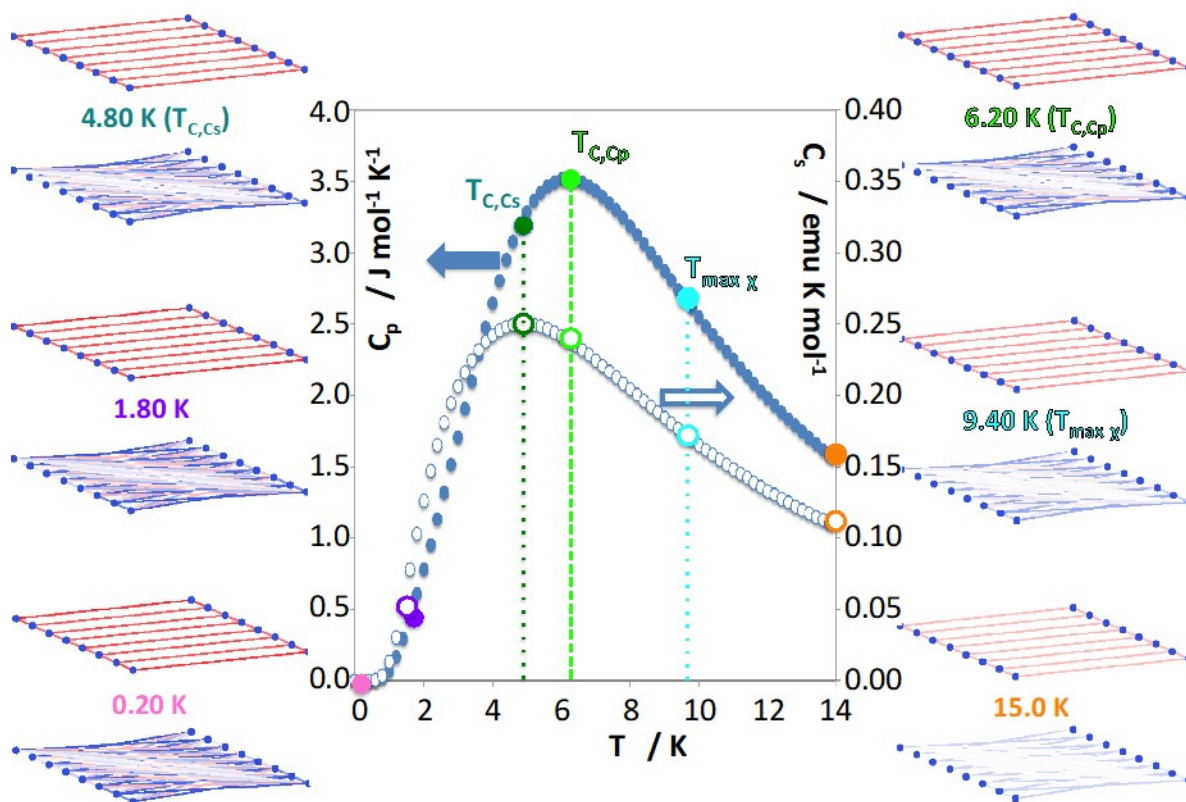

Figure SIII.4.3. Heat capacity $C_p(T)$ (solid symbol, ●) and magnetic capacity $C_s(T)$ (empty symbol, ○) as a function of temperature. See inset for temperature dependence of the magnetic correlation between all spin units at 0.2 K, 1.8 K (lowest temperature of magnetization measures), 4.8 K ($T_{C,Cs}$), 6.2 K ($T_{C,Cp}$), 9.4 K ($T_{max,\chi}$) and 15 K. Upper/lower plots represent short-/long-range spin correlation between magnetic units. Note that coupled spins are represented in red, and spins arranged parallel are shown in blue. Note also that the thickness of the lines connecting spin carriers is proportional to the strength of the correlation between spins.

Next, we will use the heat capacity, $C_p(T)$, and the magnetic capacity, $C_s(T)$, to further characterize the magnetic behavior of **2**. Heat capacity, $C_p(T)$, measures the energy variation due to the 3D propagation of the interaction of two magnetically connected spins, that is, to short-range ordering. In addition, magnetic capacity, $C_s(T)$, is a measure of the thermal variation of the spin multiplicity of the system and, thus, reflects the importance of magnetically non-connected spin alignment and how the dominant effect of long-range spin correlation governs the magnetic behavior of molecule-based crystals (and in general of magnetic compounds). It follows that the current definition of the critical temperature T_C for magnetic systems, which is associated with a maximum in the heat capacity $C_p(T)$, does not capture the magnetic nature of the system, because

it excludes long-range magnetic order. However, a maximum in the magnetic capacity $C_s(T)$, that in turn includes changes in short- and long-range spin order/disorder, is a more broadly applicable definition of the magnetic transition temperature. Also, the analysis of the behavior of the critical temperature T_C of both magnetic $C_s(T)$ and heat $C_p(T)$ capacities provides information on the importance of long-range spin correlation.

$\langle P_{ij}(J) \rangle_T$
short-range spin correlation
for ground state GS configuration (ROOT=1)

$\langle P_{ij}(0) \rangle_T$
long-range spin correlation
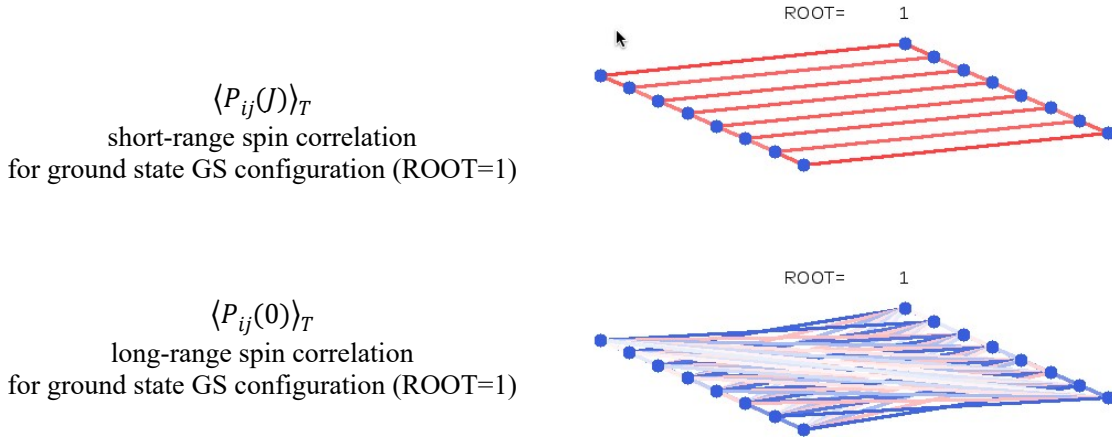for ground state GS configuration (ROOT=1)

Figure SIII.4.4. Short-range $\langle P_{ij}(J) \rangle_T$ and long-range $\langle P_{ij}(0) \rangle_T$ spin correlations for ground state GS configuration. Ground state is a singlet for **2**. Notice that coupled spins are represented in red, and spins arranged in parallel are shown in blue.

For **2**, T_C calculated from $C_p(T)$ is 6.2K and from $C_s(T)$ is 4.8K (see Figure SIII.4.3). We know that a large ratio between both critical temperatures is synonymous with magnetic topology of high dimensionality, and with importance of long-range spin ordering. The $(T_{C,Cs}/T_{C,Cp})$ ratio is 77 %, which is indicative that a 2D to 3D crossover might be feasible at low temperatures. This is in fact corroborated by the analysis of the magnetic wavefunction at different temperatures (see inset in Figure SIII.4.3), which shows large contribution of both short- and long-range spin correlation as already appraised up to 4.8K (i.e. $T_{C,Cs}$). Note that short-range spin ordering is purely AFM (i.e. antiparallel spin alignment, see red lines in Figure SIII.4.3), while long-range is mostly FM (i.e. parallel spin alignment, see blue lines in Figure SIII.4.3). From 4.8K to 6.2K (i.e. $T_{C,Cp}$), the contribution from long-range ordering becomes smaller. In fact, the no appearance of connections between spin-carrying moieties means that there is a non-ordered spin alignment (non-color lines in Figure SIII.4.3). At 9.4K ($T_{max,\chi}$), long-range order is almost lost, and at 15K it can be discarded, whereas short-range becomes less important.

Finally, comparison between the short-range $\langle P_{ij}(J)\rangle_T$ and long-range $\langle P_{ij}(0)\rangle_T$ spin correlations of the ground state of **2** shows that the singlet ground state is the collective result of singlet as well as higher multiplicity configurations (see Figure SIII.4.4).